

Accelerated Atomistic Modeling of Phase Change Memory using Deep Neural Network and Specialized Hardware

Zhuoying Zhao, Junhua Li, Pinghui Mo, Xin Zhang and Jie Liu

Abstract—Atomistic simulations offer valuable insights into phase change memory (PCM) device research and development. Current methods, such as density functional theory (DFT) and machine learning interatomic potential (ML-IAP), face limitations in device-scale modeling. DFT achieves a time-to-solution (η_t) $\approx 10^{-2}$ s/step/atom and an energy-to-solution (η_p) $\approx 10^1$ J/step/atom. State-of-the-art ML-IAPs, accelerated by GPUs, achieve $\eta_t \approx 10^{-6}$ s/step/atom and $\eta_p \approx 10^{-3}$ J/step/atom. We present a more efficient method that integrates deep neural network (DNN) with a special-purpose hardware accelerator, achieving $\eta_t \approx 10^{-7}$ s/step/atom and $\eta_p \approx 10^{-5}$ J/step/atom. Our method offers a powerful tool for high-throughput screening of PCM design possibilities (e.g., doping, interfaces), within practical time and energy consumption.

Index Terms—Phase change memory, atomistic modeling, deep learning, hardware accelerator, efficient simulation

I. INTRODUCTION

Phase change memory (PCM) has emerged as a promising candidate for next-generation non-volatile memory and neuro-inspired computing device technology [1, 2]. However, the optimizing of PCM devices requires a comprehensive understanding of their atomic-level behavior, such as electrical interface resistance and thermal boundary resistance [2]. This underscores the need for efficient and accurate atomistic modeling techniques to bridge the gap between theoretical insights and practical device performance.

Density functional theory (DFT)-based molecular dynamics (MD) have provided unparalleled accuracy in studying PCM materials [3, 4]. However, DFT involves high computational cost and poor scaling, hindering large-scale ($> 10^3$ atoms) and

This work is supported by the National Natural Science Foundation of China (#62474058, #61804049); the Fundamental Research Funds for the Central Universities of P.R. China; the YueLuShan Center for Industrial Innovation (2023YCI0104, 2025YCI0103); Huxiang High Level Talent Gathering Project (#2019RS1023); the Key Research and Development Project of Hunan Province, P.R. China (#2019GK2071); the Technology Innovation and Entrepreneurship Funds of Hunan Province, P.R. China (#2019GK5029). (Corresponding author: Jie Liu.)

Zhuoying Zhao and Junhua Li are with the College of Electrical and Information Engineering, Hunan University, Changsha 410082, China.

Pinghui Mo and Xin Zhang are with the College of Integrated Circuits, Hunan University, Changsha 410082, China.

Jie Liu is with the College of Integrated Circuits, Hunan University, Changsha 410082, China, Greater Bay Area Institute for Innovation, Hunan University, Guangzhou 511300, China, and AI for Science Institute, Beijing 100080, China (e-mail: jie_liu@hnu.edu.cn).

These authors contributed equally: Zhuoying Zhao, Junhua Li.

long-term (> 1 ns) dynamics analyses [5, 6]. Recently, machine learning interatomic potentials (ML-IAPs) have emerged as a modern alternative, adopting ML models to efficiently approximate the potential energy surface (PES). State-of-the-art ML-IAP methods in PCM research include neural network potentials (NNPs) [7], Gaussian approximation potentials (GAPs) [8], and moment tensor potentials (MTPs) [9]. However, these methods still demand substantial computational resources for large-scale atomistic simulations [10], presenting challenges in terms of cost and accessibility.

In this letter, we propose a method that combines deep neural networks (DNNs) with hardware acceleration to enable efficient and accurate atomistic modeling, addressing the limitations of existing techniques. We show that the accuracy (near-DFT level) and efficiency (orders of magnitude faster than DFT and ML-IAPs) of our approach achieves large-scale simulations with over 1.5 million atoms. This improvement paves the way for advanced studies of PCM materials and devices at previously inaccessible scales.

II. METHODOLOGY

The proposed method consists of three sequential steps. Firstly, high-fidelity training data is obtained. We generate the datasets for GeTe using DFT as implemented in CP2K [11]. The supercell contains 64 atoms, where initial $L_x=L_y=L_z=11.97$ Å. The $2\times 2\times 2$ Monkhorst-Pack k -point grid is used to sample Brillouin Zone; the Perdew-Burke-Ernzerhof (PBE) is used to account for the exchange-correlation effects [12]; the Gaussian plane wave cutoff is set to 300 Ry. The time-step is set to 5 fs; and the temperature is controlled by Nose-Hoover thermostat [13, 14]. The temperature follows a melt-quench scheme: the crystalline GeTe (*c*-GeTe) is heated from 300 K to 2000 K over 17 ps, melted into liquid GeTe (*l*-GeTe), and held at 2000 K for 10 ps. It is then cooled to 1000 K at 250 K/ps, quenched to 300 K at 25 K/ps to form amorphous GeTe (*a*-GeTe), and maintained at 300 K for 20 ps. Three melt-quench trajectories are generated, yielding 53,400 datasets, with 60% used for training and 40% for validation. The datasets for Sb and $\text{Ge}_2\text{Sb}_2\text{Te}_5$ are obtained from literatures [15, 16].

Secondly, a DNN-based potential scheme is utilized to accurately reproduce PES across different phases [17]. The DNN framework employs a symmetry-preserving embedding network with layer sizing $1\times 8\times 16\times 32$ to process each neighbor atom, followed by a fitting network with $128\times 128\times 128\times 128\times 1$ architecture to map embedded features to atomic energy. The hyperbolic tangent function ($\text{Tanh}(x)$) is

applied as the activation function in all hidden layers. The training protocol involves two stages: (1) A baseline model is first trained in FP32 format with 10 million steps using the Adam optimizer and an initial learning rate of 0.001; (2) The baseline model is then quantized (see Refs. [18-20], for quantization techniques), and fine-tuned for 10,000 steps with a reduced learning rate (10^{-7}) to recover potential accuracy loss induced by quantization, ensuring hardware-compatible efficiency without compromising predictive fidelity.

The DNN model is trained using DFT samples and subsequently deployed on a field-programmable gate array (FPGA)-based hardware accelerator. It is well known that von Neumann (vN) general-purpose central/graphics processing units (CPUs/GPUs) suffer from “memory wall” and “power wall” bottlenecks [21]. Specifically, the majority (e.g., over 90%) of the total calculation time and power is consumed in the frequent data shuttling between the processing units and storage units. To mitigate this problem, we deploy a special-purpose non von Neumann (NvN) architecture on the FPGA [18-20], as shown in Fig. 1 (a). This design enables pipelined process where each stage's output directly feeds into the next, reducing data shuttling latency and dedicating computation time solely to essential arithmetic and logical operations. We implemented it on Xilinx VU9P FPGA and presented the resource utilization in TABLE I. Moreover, each MD simulation timestep involves two main calculations: (i) PES evaluation and (ii) the other tasks such as numerical integration and thermostat. Notably, PES evaluation is computationally intensive and consumes the majority (e.g., over 99%) of computing time in large-scale simulations [22]. To accelerate it, we leverage the special-purpose NvN-based FPGA for part (i), while part (ii) is handled by a traditional vN-based CPU due to its lower computational cost but higher need for programming flexibility. This heterogeneous parallel architecture, as shown in Fig. 1 (b), could efficiently supports various MD simulations.

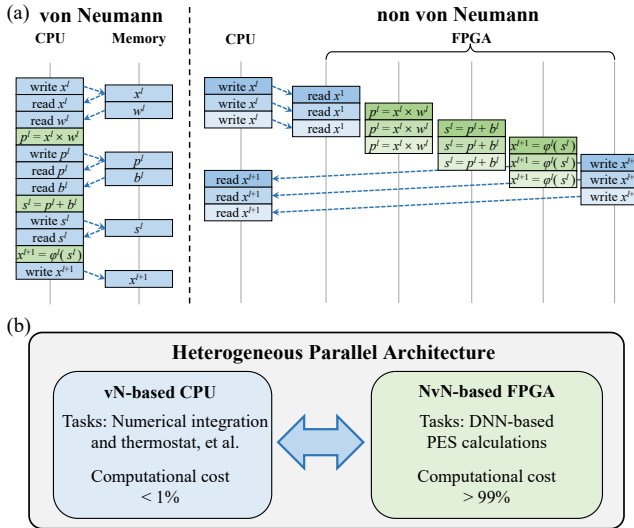


Fig. 1. (a) Comparison of calculation step between vN and NvN architecture, illustrated using the equation $x^{i+1}=\varphi(x^i \times w^i + b^i)$ for the i^{th} layer in the DNN [18-20]. (b) Schematic of the heterogeneous parallel architecture.

Critically, to enhance the computational efficiency of the overall system, a pipelined architecture is used to coordinate the execution between CPU and FPGA as shown in Fig. 1 (a). Atomic data is streamed between the CPU and FPGA, avoiding pre-storage in FPGA memory. Consequently, resource utilization in the FPGA is independent of the simulated system size, and all atoms traverse the identical computational pipeline. Meanwhile, PCIe 3.0 \times 16 interface is adopted to ensure communication time fully overlapped by FPGA computation time, preventing FPGA idle cycles. As system size increases, the communication overhead remains $O(1)$ per MD timestep (rather than $O(N)$), thereby avoiding communication bottlenecks.

TABLE I
FPGA RESOURCE UTILIZATION (XILINX VU9P DEVICE)

Resource type	Utilization	Available	Utilization rate
LUT	551,738	1,182,240	46.7%
FF	1,178,658	2,364,480	49.8%
DSP	3,253	6,840	47.6%
BRAM	550	2,160	25.5%
URAM	369	960	38.4%

Thirdly, adopting the IAP model described above, MD simulations are performed using the LAMMPS software [23]. This is achieved by substituting the force field in the LAMMPS package's input file with our developed model.

III. RESULTS

We use the method proposed in Section II to simulate the melt-quench-anneal process for the elementary system Sb, the binary systems GeTe, and the ternary system Ge₂Sb₂Te₅. The crystalline structures are constructed with size of $36 \times 31 \times 47 \text{ nm}^3$ (1,536,000 atoms) for Sb, $37 \times 37 \times 37 \text{ nm}^3$ (1,728,000 atoms) for GeTe, and $33 \times 38 \times 44 \text{ nm}^3$ (1,687,500 atoms) for Ge₂Sb₂Te₅. The time-step is set as 2 fs, and Canonical ensemble (i.e., NVT) MD is performed.

TABLE II compares the computational efficiency of different methods in terms of time-to-solution (η_t) and energy-to-solution (η_p). Our method, implemented on a single Xilinx VU9P FPGA, demonstrates improvements across all tested systems. Benchmarked against DFT running on dual-socket Intel 8375C CPUs, our method reduces η_t by 5 orders of magnitude and η_p by 6 orders of magnitude. Even against ML-IAP accelerated by an NVIDIA V100 GPU, it achieves 1 order of magnitude faster and 2 orders of magnitude more energy-efficient. Notably, our method shows superior scalability, successfully handling system sizes over 1.5 million atoms, which is approximately 19 \times larger than the maximum system size achievable by GPU-accelerated ML-IAPs.

Recently, ref. [10] reported an ML-IAP model simulating a memory bit with size of $20 \times 20 \times 40 \text{ nm}^3$ (532,980 atoms), achieving $\eta_t \approx 10^{-5} \text{ s/step/atom}$ and $\eta_p \approx 10^{-1} \text{ J/step/atom}$ using thousands of CPU cores. These efficiency metrics were derived from computational parameters (hardware configuration, wall time, etc.) provided by the authors of Ref. [10]. In contrast, our method simulates systems 3 \times larger on a single FPGA, while reducing η_t by 2 orders of magnitude and

η_p by 4 orders of magnitude. This scalability underscores our method's potential to address larger device geometries and extended simulation timescales, critical for optimizing PCM device parameters such as doping concentrations and interface dynamics.

TABLE II
COMPARISON OF TIME-TO-SOLUTION AND ENERGY-TO-SOLUTION OF DIFFERENT METHODS

Method	System	Atoms number	Time-to-solution η_t (s-step ⁻¹ .atom ⁻¹)	Energy-to-solution η_p (J-step ⁻¹ .atom ⁻¹)
DFT based on CPU	Sb	192	6.7×10^{-2}	5.4×10^1
	GeTe	216	4.9×10^{-2}	3.9×10^1
	Ge ₂ Sb ₂ Te ₅	108	5.3×10^{-2}	4.2×10^1
ML-IAP based on GPU	Sb	81,000	2.7×10^{-6}	1.6×10^{-3}
	GeTe	86,400	2.9×10^{-6}	1.7×10^{-3}
	Ge ₂ Sb ₂ Te ₅	86,400	3.3×10^{-6}	2.0×10^{-3}
this work based on FPGA	Sb	1,536,000	1.7×10^{-7}	3.8×10^{-5}
	GeTe	1,728,000	2.8×10^{-7}	6.1×10^{-5}
	Ge ₂ Sb ₂ Te ₅	1,687,500	2.7×10^{-7}	6.3×10^{-5}

The proposed method demonstrates high accuracy while achieving high efficiency. As shown in Fig. 2, the computed energy and atomic force in this work are in satisfactory agreement with DFT results. Specifically, the root-mean-square error (RMSE) for energy prediction is $\|e_E\|_2 = 4.95$, 7.51, 17.47 meV/atom; and the RMSE for atomic force prediction is $\|e_F\|_2 = 86.98$, 149.63, 130.59 meV/Å, for Sb, GeTe and Ge₂Sb₂Te₅, respectively. Notably, $\|e_E\|_2$ here (10^{-3} – 10^{-2} eV/atom) is 2–3 orders of magnitude smaller than typical interatomic bond energy (10^0 – 10^1 eV/atom [24]), and well below the chemical accuracy threshold (1.0 kcal mol⁻¹, i.e., 43.4 meV/atom [25]). While force RMSEs for GeTe and Ge₂Sb₂Te₅ exceed Sb's, they are comparable/superior to prior ML-IAPs (Sb: 64.19 meV/Å [15]; GeTe: 170 meV/Å [26]; Ge₂Sb₂Te₅: 159 meV/Å [16]), indicating decent accuracy of the proposed method.

To assess phase-specific accuracy, we analyzed GeTe system. The energy/force RMSEs are: crystalline (5.09 meV/atom, 108.15 meV/Å), liquid (10.43 meV/atom, 197.63 meV/Å), and amorphous (7.24 meV/atom, 152.62 meV/Å). The model shows better accuracy in crystalline phases due to ordered atomic configurations, while liquid phases exhibit higher errors from thermal fluctuations at elevated temperatures. Despite these variations, structural fidelity remains robust across all phases (Fig. 3-4).

The local structures of the liquid/amorphous phases for Sb, GeTe and Ge₂Sb₂Te₅ have been obtained at temperatures of 1200K/300K, 1200K/300K and 990K/300K, respectively. These results are compared with DFT at the same temperature [15, 16, 26]. The radial distribution functions (RDFs), shown in Fig. 3, demonstrate excellent agreement with DFT results. Furthermore, the Peierls distortion, a subtle structural feature in PCMs that plays an important role in tuning electronic bandgap [27], is accurately evaluated using the angular-limited three-body correlation (ALTBC) function. As depicted in Fig. 4, our method successfully captures this effect in *a*-

GeTe, aligning closely with DFT results and prior study [28], validating its ability to describe structural properties.

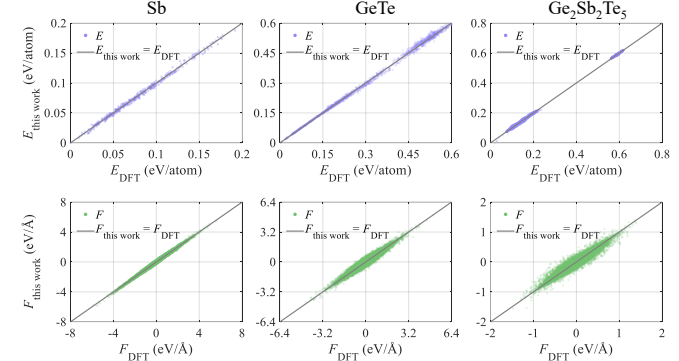


Fig. 2. Comparison of predicted energy and force. The energy/force predicted by the proposed method ($E_{\text{this work}}/E_{\text{DFT}}$) are compared with those computed using DFT ($E_{\text{DFT}}/E_{\text{DFT}}$).

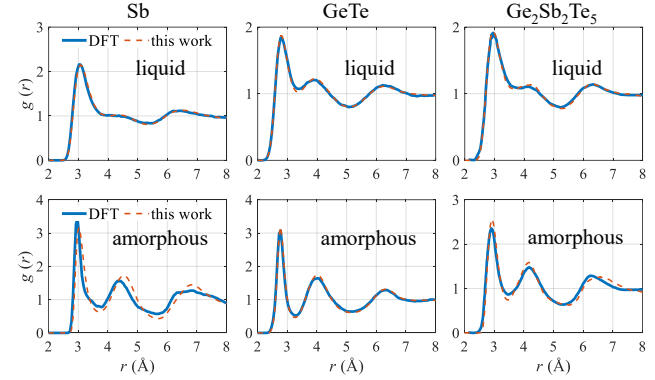


Fig. 3. Radial distribution functions (RDFs) of *I*-Sb/*a*-Sb at 1200 K/300 K, *I*-GeTe/*a*-GeTe at 1200 K/300 K, and *I*-Ge₂Sb₂Te₅/*a*-Ge₂Sb₂Te₅ at 990 K/300 K. The DFT results are obtained from ref. [15, 16, 26].

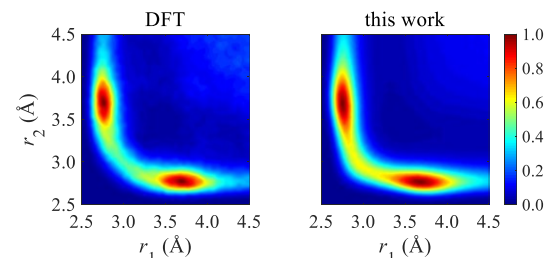


Fig. 4 The degree of Peierls distortion evaluated by ALTBC of *a*-GeTe at 300K. Results from this work (1,728,000-atom) and DFT (216-atom) are compared.

IV. DISCUSSION

The accuracy, efficiency and scalability of the proposed method open avenues for optimizing PCM devices. For example, our method may be useful for directly modeling dopant-suppressed resistance drift and phase separation phenomena in PCM. In addition, it could be used to study defect propagation and thermal boundary resistance at realistic scales within a feasible time frame. This capability addresses a key gap in current PCM research, where device-level insights require atomic-scale resolution at previously inaccessible scales. Currently, an FPGA cloud platform has been

established [29], which is accessible at for researchers to utilize computational resources. Moreover, we are migrating this acceleration work to ASIC to further improve computational efficiency. Due to ASIC's higher clock frequency and more hardware resources compared to FPGA, ASIC is expected to enhance computational speed by another two orders of magnitude [20].

While the propose method enables large-scale and efficient modeling, their extension to novel PCM compositions requires addressing technical considerations. Although the DNN framework our used is universally applicable to different PCM materials (e.g., Sb, GeTe, Ge₂Sb₂Te₅), it requires material-specific retraining. Crucially, our FPGA accelerator supports flexible parameter reconfiguration. When transitioning to new materials, the CPU transfers updated DNN weights to the FPGA's memory without hardware redesign. However, the model's accuracy fundamentally depends on the quality of the training data quality. Insufficient coverage of atomic configurations may limit prediction fidelity for target phenomena. Fortunately, recent advances in pre-trained large atomic model (LAM) show promise. For instance, the DPA-2 model introduced in Ref. [30] demonstrates exceptional generalization capability through large-scale multi-task pre-training across diverse datasets. This approach achieves a 1–2 order-of-magnitude reduction in data requirements without sacrificing accuracy. We will actively contribute to the development of such universal models and integrate them with our dedicated hardware accelerators in future work to further enhance scalability and efficiency.

V. CONCLUSION

This work presents a high-efficiency atomistic modeling method for PCM that achieves DFT-level accuracy while reducing the time-to-solution to 10⁻⁷ s/step/atom and the energy-to-solution to 10⁻⁵ J/step/atom. This performance improvement is enabled by the tight integration of deep neural network and specialized hardware acceleration. Validated through million-atom simulations of Sb, GeTe, and Ge₂Sb₂Te₅ systems, our method shows the potential to explore complex PCM systems and phenomena within feasible timeframes. Such capability addresses the growing need for cross-scale simulation tools in PCM device research and development.

REFERENCES

- [1] W. Zhang, R. Mazzarello, M. Wuttig, and E. Ma, "Designing crystallization in phase-change materials for universal memory and neuro-inspired computing," *Nature Reviews Materials*, vol. 4, no. 3, pp. 150-168, 2019/03/01 2019, doi: [10.1038/s41578-018-0076-x](https://doi.org/10.1038/s41578-018-0076-x).
- [2] H. S. P. Wong, S. Raoux, S. Kim, J. Liang, J. P. Reifenberg, B. Rajendran, M. Asheghi, and K. E. Goodson, "Phase Change Memory," *Proceedings of the IEEE*, vol. 98, no. 12, pp. 2201-2227, 2010, doi: [10.1109/JPROC.2010.2070050](https://doi.org/10.1109/JPROC.2010.2070050).
- [3] J. Liu, X. Xu, L. Brush, and M. P. Anantram, "A multi-scale analysis of the crystallization of amorphous germanium telluride using ab initio simulations and classical crystallization theory," *Journal of Applied Physics*, vol. 115, no. 2, p. 023513, 2014, doi: [10.1063/1.4861721](https://doi.org/10.1063/1.4861721).
- [4] F. Rao, K. Ding, Y. Zhou, Y. Zheng, M. Xia, S. Lv, Z. Song, S. Feng, I. Ronneberger, R. Mazzarello, W. Zhang, and E. Ma, "Reducing the stochasticity of crystal nucleation to enable subnanosecond memory writing," *Science*, vol. 358, no. 6369, pp. 1423-1427, 2017/12/15 2017, doi: [10.1126/science.aao3212](https://doi.org/10.1126/science.aao3212).
- [5] J. Liu, B. Yu, and M. P. Anantram, "Scaling Analysis of Nanowire Phase-Change Memory," *IEEE Electron Device Letters*, vol. 32, no. 10, pp. 1340-1342, 2011, doi: [10.1109/LED.2011.2162390](https://doi.org/10.1109/LED.2011.2162390).
- [6] Y. Xu, Y. Zhou, X.-D. Wang, W. Zhang, E. Ma, V. L. Deringer, and R. Mazzarello, "Unraveling Crystallization Mechanisms and Electronic Structure of Phase-Change Materials by Large-Scale Ab Initio Simulations," *Advanced Materials*, vol. 34, no. 11, p. 2109139, 2022/03/01 2022, doi: [10.1002/adma.202109139](https://doi.org/10.1002/adma.202109139).
- [7] G. C. Sosso, G. Miceli, S. Caravati, J. Behler, and M. Bernasconi, "Neural network interatomic potential for the phase change material GeTe," *Physical Review B*, vol. 85, no. 17, p. 174103, 05/04/ 2012, doi: [10.1103/PhysRevB.85.174103](https://doi.org/10.1103/PhysRevB.85.174103).
- [8] A. P. Bartók, M. C. Payne, R. Kondor, and G. Csányi, "Gaussian approximation potentials: The accuracy of quantum mechanics, without the electrons," *Physical review letters*, vol. 104, no. 13, p. 136403, 2010, doi: [10.1103/PhysRevLett.104.136403](https://doi.org/10.1103/PhysRevLett.104.136403).
- [9] A. V. Shapeev, "Moment tensor potentials: A class of systematically improvable interatomic potentials," *Multiscale Modeling & Simulation*, vol. 14, no. 3, pp. 1153-1173, 2016, doi: [10.1137/15M1054183](https://doi.org/10.1137/15M1054183).
- [10] Y. Zhou, W. Zhang, E. Ma, and V. L. Deringer, "Device-scale atomistic modelling of phase-change memory materials," *Nature Electronics*, vol. 6, no. 10, pp. 746-754, 2023/10/01 2023, doi: [10.1038/s41928-023-01030-x](https://doi.org/10.1038/s41928-023-01030-x).
- [11] J. VandeVondele, M. Krack, F. Mohamed, M. Parrinello, T. Chassaing, and J. Hutter, "Quickstep: Fast and accurate density functional calculations using a mixed Gaussian and plane waves approach," *Computer Physics Communications*, vol. 167, no. 2, pp. 103-128, 2005/04/15 2005, doi: [10.1016/j.cpc.2004.12.014](https://doi.org/10.1016/j.cpc.2004.12.014).
- [12] J. P. Perdew, K. Burke, and M. Ernzerhof, "Generalized Gradient Approximation Made Simple," *Physical Review Letters*, vol. 77, no. 18, pp. 3865-3868, 10/28/ 1996, doi: [10.1103/PhysRevLett.77.3865](https://doi.org/10.1103/PhysRevLett.77.3865).
- [13] S. Nosé, "A unified formulation of the constant temperature molecular dynamics methods," *The Journal of Chemical Physics*, vol. 81, no. 1, pp. 511-519, 1984, doi: [10.1063/1.447334](https://doi.org/10.1063/1.447334).
- [14] W. G. Hoover, "Canonical dynamics: Equilibrium phase-space distributions," *Physical Review A*, vol. 31, no. 3, pp. 1695-1697, 03/01/ 1985, doi: [10.1103/PhysRevA.31.1695](https://doi.org/10.1103/PhysRevA.31.1695).
- [15] M. Shi, J. Li, M. Tao, X. Zhang, and J. Liu, "Artificial intelligence model for efficient simulation of monatomic phase change material antimony," *Materials Science in Semiconductor Processing*, vol. 136, p. 106146, 2021, doi: [10.1016/j.mssp.2021.106146](https://doi.org/10.1016/j.mssp.2021.106146).
- [16] O. Abou El Kheir, L. Bonati, M. Parrinello, and M. Bernasconi, "Unraveling the crystallization kinetics of the Ge₂Sb₂Te₅ phase change compound with a machine-learned interatomic potential," *npj Computational Materials*, vol. 10, no. 1, p. 33, 2024, doi: [10.1038/s41524-024-01217-6](https://doi.org/10.1038/s41524-024-01217-6).
- [17] L. Zhang, J. Han, H. Wang, W. A. Saidi, R. Car, and E. Weinan, "End-to-end symmetry preserving inter-atomic potential energy model for finite and extended systems," presented at the Proceedings of the 32nd International Conference on Neural Information Processing Systems, Montréal, Canada, 2018, doi: [10.5555/3327345.3327356](https://doi.org/10.5555/3327345.3327356).
- [18] P. Mo, C. Li, D. Zhao, Y. Zhang, M. Shi, J. Li, and J. Liu, "Accurate and efficient molecular dynamics based on machine learning and non von Neumann architecture," *npj Computational Materials*, vol. 8, no. 1, p. 107, 2022/05/09 2022, doi: [10.1038/s41524-022-00773-z](https://doi.org/10.1038/s41524-022-00773-z).
- [19] Z. Zhao, Z. Tan, P. Mo, X. Wang, D. Zhao, X. Zhang, M. Tao, and J. Liu, "A Heterogeneous Parallel Non-von Neumann Architecture System for Accurate and Efficient Machine Learning Molecular Dynamics," *IEEE Transactions on Circuits and Systems I: Regular Papers*, vol. 70, no. 6, pp. 2439-2449, 2023, doi: [10.1109/TCSI.2023.3255199](https://doi.org/10.1109/TCSI.2023.3255199).
- [20] P. Mo, Y. Zhang, Z. Zhao, H. Sun, J. Li, D. Guan, X. Ding, X. Zhang, B. Chen, and M. Shi, "High-speed and low-power molecular dynamics processing unit (MDPU) with ab initio accuracy," *npj Computational Materials*, vol. 10, no. 1, p. 253, 2024, doi: [10.1038/s41524-024-01422-3](https://doi.org/10.1038/s41524-024-01422-3).
- [21] W. A. Wulf and S. A. McKee, "Hitting the memory wall: implications of the obvious," *SIGARCH Comput. Archit. News*, vol. 23, no. 1, pp. 20–24, 1995, doi: [10.1145/216585.216588](https://doi.org/10.1145/216585.216588).
- [22] D. Lu, H. Wang, M. Chen, J. Liu, L. Lin, R. Car, E. Weinan, W. Jia, and L. Zhang, "86 PFLOPS Deep Potential Molecular Dynamics simulation of 100 million atoms with ab initio accuracy," *Comput. Phys. Commun.*, vol. 259, p. 107624, 2020, doi: [10.1016/J.CPC.2020.107624](https://doi.org/10.1016/J.CPC.2020.107624).
- [23] S. Plimpton, "Fast Parallel Algorithms for Short-Range Molecular Dynamics," *Journal of Computational Physics*, vol. 117, no. 1, pp. 1-19, 1995/03/01/ 1995, doi: [10.1006/jcph.1995.1039](https://doi.org/10.1006/jcph.1995.1039).

- [24] R. T. Sanderson, "Interrelation of bond dissociation energies and contributing bond energies," *Journal of the American Chemical Society*, vol. 97, no. 6, pp. 1367-1372, 1975/03/01 1975, doi: [10.1021/ja00839a013](https://doi.org/10.1021/ja00839a013).
- [25] J. A. Pople, "Nobel Lecture: Quantum chemical models," *Reviews of Modern Physics*, vol. 71, no. 5, pp. 1267-1274, 10/01/ 1999, doi: [10.1103/RevModPhys.71.1267](https://doi.org/10.1103/RevModPhys.71.1267).
- [26] M. Shi, P. Mo, and J. Liu, "Deep Neural Network for Accurate and Efficient Atomistic Modeling of Phase Change Memory," *IEEE Electron Device Letters*, vol. 41, no. 3, pp. 365-368, 2020, doi: [10.1109/LED.2020.2964779](https://doi.org/10.1109/LED.2020.2964779).
- [27] J. Y. Raty, W. Zhang, J. Luckas, C. Chen, R. Mazzarello, C. Bichara, and M. Wuttig, "Aging mechanisms in amorphous phase-change materials," *Nature Communications*, vol. 6, no. 1, p. 7467, 2015/06/24 2015, doi: [10.1038/ncomms8467](https://doi.org/10.1038/ncomms8467).
- [28] W. Zhang and E. Ma, "Unveiling the structural origin to control resistance drift in phase-change memory materials," *Materials Today*, vol. 41, pp. 156-176, 2020/12/01/ 2020, doi: [10.1016/j.mattod.2020.07.016](https://doi.org/10.1016/j.mattod.2020.07.016).
- [29] <http://nvnmd.picp.vip>.
- [30] D. Zhang, X. Liu, X. Zhang, C. Zhang, C. Cai, H. Bi, Y. Du, X. Qin, A. Peng, J. Huang, B. Li, Y. Shan, J. Zeng, Y. Zhang, S. Liu, Y. Li, J. Chang, X. Wang, S. Zhou, J. Liu, X. Luo, Z. Wang, W. Jiang, J. Wu, Y. Yang, J. Yang, M. Yang, F.-Q. Gong, L. Zhang, M. Shi, F.-Z. Dai, D. M. York, S. Liu, T. Zhu, Z. Zhong, J. Lv, J. Cheng, W. Jia, M. Chen, G. Ke, W. E, L. Zhang, and H. Wang, "DPA-2: a large atomic model as a multi-task learner," *npj Computational Materials*, vol. 10, no. 1, p. 293, 2024/12/19 2024, doi: [10.1038/s41524-024-01493-2](https://doi.org/10.1038/s41524-024-01493-2).